Solid-State NMR, Ionic Conductivity, and Thermal Studies of Lithium-doped Siloxane−Poly(propylene glycol) Organic−Inorganic Nanocomposites

Paulo H. de Souza,[†,‡] Rodrigo F. Bianchi,[†] Karim Dahmouche,[†,§] Patrick Judeinstein,[∥] Roberto M. Faria,[†] and Tito J. Bonagamba*[,†]

Instituto de Física de São Carlos, Universidade de São Paulo, Caixa Postal 369, CEP 13560-970, São Carlos-SP, Brazil, and Laboratoire de Chimie Structurale Organique, and UPRESA CNRS 8074, Université Paris-Sud, 91405 Orsay, France

Received February 1, 2001

Hybrid organic−inorganic ionic conductors, also called ormolytes (*or*ganically *mo*dified electro*lytes*), were obtained by dissolution of $LiClO_4$ in siloxane−poly(propylene glycol) matrixes. The dynamic features of these nanocomposites were studied and correlated to their electrical properties. Solid-state nuclear magnetic resonance (NMR) spectroscopy was used to probe the effects of the temperature and nanocomposite composition on the dynamic behaviors of both the ionic species (^{7}Li) and the polymer chains (^{13}C). NMR, dc ionic conductivity, and DSC results demonstrate that the Li^+ mobility is strongly assisted by the segmental motion of the polymer chain above its glass transition temperature. The ac ionic conductivity in such composites is explained by use of the random free energy barrier (RFEB) model, which is in agreement with their disordered and heterogeneous structures. These solid ormolytes are transparent and flexible, and they exhibit good ionic conductivity at room temperature (up to 10^{-4} S/cm). Consequently, they are very promising candidates for use in several applications such as batteries, sensors, and electrochromic and photoelectrochemical devices.

Introduction

In recent years, the sol−gel method has successfully been used for the production of a significant number of novel organic−inorganic frameworks with tunable designs and suitable properties.[1−7] The combination of appropriate processing conditions with adequate choice for the organic and inorganic components dictates the morphology, molecular structure, and features of the resulting materials. The intense activity in this domain of research is due to the extraordinary implications that derive from the possibility of tailoring multifunctional advanced compounds by mixing organic and inorganic components at the nanosize level in a single material.[1−7] The synergy of that combination and the particular role of the inner organic−inorganic interfaces enlarge the scope of application of nanohybrid materials in areas such as electrochemistry, biology, mechanics, ceramics, electronics, and optics.[4−7] The hybrid concept seems to be particularly well-adapted for the production of advanced solid materials presenting ion-conducting properties, with the advantage of replacing viscous liquid systems by solid or rubbery materials.[8,9] These solid polymer electrolytes, so-called ormolytes (*or*ganically *mo*dified electro*lytes*), are very promising because of their possible use in various applications such as batteries, data storage, sensors, and electrochromic and photoelectrochemical devices.[9−11] Among the various organic−inorganic hybrids that have been proposed in the past several years, a family of versatile compounds, classified as di-ureasils, in which polyether- [poly(propylene glycol)- (PPG-) or poly(ethylene glycol)- (PEG-)] based chains of variable length are grafted on both ends to a siliceous backbone through urea functionalities, is noteworthy.[8,12−14] When doped with lithium salts, these solid, transparent, and flexible nanocomposites exhibit good ionic conductivity at room temperature (up to 10^{-6} S/cm).[15−18] Because of the presence of

* Author to whom correspondence should be addressed. Tito J. Bonagamba, Instituto de Física de São Carlos, Universidade de São Paulo, Caixa Postal 369, CEP 13560-970, São Carlos-SP, Brazil. E-mail: tito@if.sc.usp.br.

† Universidade de São Paulo.

‡ Present address: Centro Federal de Educação Tecnológica de Goiás, UNED/Jataí, Rua Riachuelo, 2090 − Setor Manuel Graham, CEP: 13580−000, Jataí-GO (Brazil).

§ Present address: Instituto de Química de Araraquara−UNESP, Av. Prof. Francisco Degni s/n, CEP 14800-900, Araraquara-SP, Brazil.

∥ Université Paris-Sud.

(1) Brinker, J. C. *Sol−Gel Science, The Physics and Chemistry of Sol−Gel Processing*; Academic Press: New York, 1989.

(2) Uhlmann, D. R.; Ulrich, D. R. *Ultrastructure Processing of Advanced Materials*; Wiley: New York, 1992.

(3) Hench, L. L.; West, J. K. *Chemical Processing of Advanced Materials*; Wiley: New York, 1992.

(4) Mark, J. E., Lee, C. C-Y., Bianconi, P. A., Eds. *Hybrid Organic−Inorganic Composites*; ACS Symposium Series No. 585; American Chemical Society: Washington, D.C., 1995.

(5) Klein, L. C. *Sol−Gel Technology for Thin Films, Fiber, Preforms, Electronics and Speciality Shapes*; Noyes: Park Ridge, NJ, 1988.

(6) Judeinstein, P.; Sanchez, C. J. *J. Mater. Chem.* **1996**, *6*, 511−525.

(7) Sanchez, C.; Ribot, F.; Lebeau, B. *J. Mater. Chem.* **1999**, *9*, 35−44.

(8) Bermudez, V. Z.; Poinsignon, C.; Armand, M. *J. Mater. Chem.* **1997**, *7*, 1677−1692.

(9) Judeinstein, P.; Livage, J.; Zarudiansky, A.; Rose, R. *Solid State Ionics* **1988**, *28*, 1722−1725.

(10) Armand, M. *Adv. Mater.* **1990**, *2*, 278−286.

(11) Orel, B.; Krasovec, U. O.; Stangar, U. L. *J. Sol−Gel Sci. Technol.* **1998**, *11*, 87−104.

(12) Ravaine, D.; Seminel, A.; Charbouillot, Y.; Vincens, M. *J. Non-Cryst. Solids* **1986**, *82*, 210−219.

10.1021/cm011023v CCC: $20.00 © 2001 American Chemical Society
Published on Web 09/28/2001

covalent bonds between the inorganic (siloxane) and organic (polymer) phases, these hybrids (classified as type II[4,6,7]) have higher chemical stabilities and better mechanical properties than pure organic polymers.[12−14] Siloxane−polyether ormolytes presenting only weak physical bonds (hydrogen bridges or van der Waals bonds) between the inorganic and organic phases (type I) have also been obtained.[15−19] These rubbery blends have higher room-temperature ionic conductivities (up to 10^{-4} S/cm) than the type II hybrids but much lower chemical stabilities.

In recent works,[19−22] the structural and dynamical properties of siloxane−PEG lithium-doped ormolytes have been correlated with their ion-conduction mechanisms. It was shown[22] that, as observed for pure organic polymers,[23−25] conductivity occurs in the amorphous phase above the glass transition temperature T_g via a liquidlike motion of the cations associated with segmental reorientations of the neighboring chains. Therefore, electrical properties are strongly dependent on the mobilities of both the polymer chains and the active ionic species, which are themselves dependent on the synthesis conditions such as the polymer molecular weight, the lithium concentration, the weight percent of polymer, and the interactions between the organic and inorganic phases.[19−22]

The effects of the synthesis conditions on the dynamic properties of siloxane−PPG nanocomposites are still not completely known. The optimization of the properties of these nanocomposites should take into consideration information about their microscopic molecular behavior, and for this purpose, nuclear magnetic resonance (NMR) spectroscopy can make important contributions. This work reports a ^{7}Li and ^{13}C solid-state NMR study of hybrid ionic conductors based on siloxane−PPG networks of types I and II doped with lithium perchlorate ($LiClO_4$). NMR spectroscopy was used to study both the cation ($^7Li^+$) and the polymer backbone (^{13}C) mobilities through measurements of line widths, $\Delta\nu$, and spin−lattice relaxation times, T_1, as functions of temperature.

Table 1. Ormolytes of Types I and II and Lithium-Silica-free Samples

series 1	series 2	series 3	series 4	series 5
$[67]_7$[4]-I	$[74]_5$[4]-II	$[95]_{34}$[4]-II	$[97]_{69}$[4]-II	$[100]_{69}[\infty]$
$[67]_7$[8]-I	−	$[95]_{34}$[8]-II	$[97]_{69}$[8]-II	−
$[67]_7$[10]-I	−	$[95]_{34}$[10]-II	$[97]_{69}$[15]-II	−
$[67]_7$[15]-I	−	$[95]_{34}$[15]-II	−	−
$[67]_7$[20]-I	−	$[95]_{34}$[20]-II	−	−
$[67]_7$[30]-I	−	$[95]_{34}$[30]-II	−	−
$[67]_7$[80]-I	−	$[95]_{34}$[80]-II	−	−

Differential scanning calorimetry (DSC) was used to identify the glass transition temperature, and ionic conductivity results were included for further discussion and elucidation of the influence of the material composition on their properties.

Materials

Sample Preparation. All chemical reagents are commercially available (Fluka, Aldrich) and were used without further purification and isotopic enrichment. Type I hybrids were prepared by an ultrasonic method[15−18] in which 12.5 mL of tetraethoxysilane (TEOS) and 4 mL of water were stirred together under ultrasound to hydrolyze the TEOS. Then, the desired quantities of the viscous poly(propylene glycol), $HO(CH_2CH(CH_3)O)_nH$ (PPG), with various molecular weights were added under neutral pH conditions. $LiClO_4$ was then introduced and dissolved using ultrasound to obtain a transparent monophasic liquid. Gelation occurred in a few minutes, and the obtained product was slowly dried at 90 °C resulting in a monolithic solid piece. This method is very similar to the procedure used previously[13,26] to prepare type I nanocomposites containing poly(ethylene glycol), $HO(CH_2CH_2O)_nH$ (PEG), with the exception of the ultrasonic activation. In these materials, only weak interactions are expected to link together the organic and inorganic components.[13,19,26]

Type II siloxane−PPG hybrids were obtained by mixing equimolar amounts of 3-isocyanatopropyltriethoxysilane (IsoTrEOS) and O,O′-bis(2-aminopropyl)poly(propylene glycol) [abbreviated $NH_2-(PPG)_n-NH_2$], which were stirred together in tetrahydrofuran (THF) and refluxed for 6 h. THF was evaporated, and the pure hybrid precursor $(OEt)_3Si(PPG)_nSi(OEt)_3$ was obtained. Then, 0.5 g of this precursor was mixed with 1 mL of ethanol containing NH_4F ($NH_4F/Si = 0.005$) to which was added the desired quantity of $LiClO_4$. Finally, 0.2 mL of water was added under vigorous stirring. A monolithic gel was obtained after 4 h. The ethanol was then slowly removed under vacuum at 90 °C to yield a rubbery material. The existence of covalent chemical bonds between the silica network and the polymer chains has been reported in similar materials containing PEG.[12−14]

Immediately after the preparation and drying procedures, the nanocomposites were sealed in appropriate glass tubes for NMR experiments or in aluminum pans for DSC runs.

The following nomenclature will be used to describe the composites: $[X]_n[Y]$-Z, where X represents the weight percent of polymer, n the polymerization degree, Y the [O]/[Li] (where the oxygen atoms considered are only those of the ether group), and Z the type of ormolyte (I or II). Several samples were prepared as listed in Table 1. Series 1 is composed of nonbonded samples (type I) having different Y values, wheras series 2−4 consist of bonded samples (type II) having different combinations of X, n, and Y. The values of X and n in type II nanocomposites are codependent. Finally, series 5 consists of a lithium- and silica-free sample.

Experimental Techniques

Solid-State NMR Spectroscopy. ^{7}Li ($I = {}^3/_2$) and ^{13}C ($I = {}^1/_2$) NMR measurements were performed as a function of the

(13) Judeinstein, P.; Brik, M. E.; Bayle, J. P.; Courtieu, J.; Rault, J. *Mater. Res. Soc. Symp. Proc.* **1994**, *346*, 937−942.
(14) Brik, M. E.; Titman, J. J.; Bayle, J. P.; Judeinstein, P. *J. Polym. Sci. B: Polym. Phys.* **1996**, *34*, 2533−2542.
(15) Dahmouche, K.; Atik, M.; Mello, N. C.; Bonagamba, T. J.; Panepucci, H.; Aegerter, M. A.; Judeinstein, P. *Mater. Res. Soc. Symp. Proc.* **1996**, *435*, 363−368.
(16) Dahmouche, K.; Atik, M.; Mello, N. C.; Bonagamba, T. J.; Panepucci, H.; Aegerter, M. A.; Judeinstein, P. *J. Sol−Gel Sci. Technol.* **1997**, *8*, 711−715.
(17) Dahmouche, K.; Atik, M.; Mello, N. C.; Bonagamba, T. J.; Panepucci, H.; Judeinstein, P.; Aegerter, M. A. *Sol. Energy Mater. Sol. Cells* **1998**, *54*, 1.
(18) Dahmouche, K.; Souza, P. H.; Bonagamba, T. J.; Panepucci, H.; Judeinstein, P.; Pulcinelli, S. H.; Santilli, C. V. *J. Sol−Gel Sci. Technol.* **1998**, *13*, 909−913.
(19) Judeinstein, P.; Titman, J.; Stamm, M.; Schmidt, H. *Chem. Mater.* **1994**, *6*, 127−134.
(20) Dahmouche, K.; Santilli, C. V.; Pulcinelli, S. H.; Craievich, A. F. *J. Phys. Chem. B* **1999**, *103*, 4937−4942.
(21) Dahmouche, K.; Santilli, C. V.; Da Silva, M.; Ribeiro, C. A.; Pulcinelli, S. H.; Craievich, A. F. *J. Non-Cryst. Solids* **1999**, *247*, 108−113.
(22) Mello, N. C.; Bonagamba, T. J.; Panepucci, H.; Dahmouche, K.; Judeinstein, P.; Aegerter M, A. *Macromolecules* **2000**, *33*, 1280−1288.
(23) Gray, F. M. *Solid Polymer Electrolytes, Fundamentals and Technological Applications*, 1st ed.; VCH Publishers: New York, 1991.
(24) Lightfoot, P.; Mehta, M. A.; Bruce, P. G. *J. Mater. Chem.* **1992**, *2*, 139−140.
(25) Lightfoot, P.; Mehta, M. A.; Bruce, P. G. *Science* **1993**, *262*, 883−885.
(26) Lesot, P.; Chapuis, S.; Bayle, J. P.; Rault, J.; Lafontaine, E.; Campero, A.; Judeinstein, P. *J. Mater. Chem.* **1998**, *8*, 147−151.

temperature with the purpose of establishing relationships between the sample preparation conditions and the dynamic properties of both the Li^+ ion and the polymer chain. Solid-state NMR spectra were recorded between −100 and 140 °C in two NMR spectrometers, at 2 and 9.4 T, using Tecmag LIBRA and Varian INOVA systems, respectively. In both cases, variable-temperature double-resonance static Doty probes were employed. The Larmor frequencies are 21.4 and 33.1 MHz for ^{13}C and ^7Li, respectively, at 2 T and 155.4 MHz for ^7Li at 9.4 T. At 2 T, in all cases, the spectra were obtained from the Fourier transform of the free induction decays (FIDs) following a single 8-μs $\pi/2$ excitation and a dead time of 10 μs. For ^{13}C spectra, proton decoupling was always used during acquisition, whereas ^7Li spectra were successively acquired with and without proton decoupling. At 9.4 T, ^7Li spectra were obtained with application of the solid-echo pulse sequence[27] using two 4-μs $\pi/2$ RF pulses ($\pi/2_x-\tau-\pi/2_y$).

The full width at half-height of the ^7Li and ^{13}C lines will be defined as line width, $\Delta\nu$, in this article. The spin−lattice relaxation times T_1 were measured for ^7Li by the inversion−recovery method ($\pi-\tau_1-\pi/2$)[27] in the 2-T spectrometer. ^1H decoupling was used only during the ^7Li FID acquisition to improve the signal-to-noise ratio, thus allowing T_1 measurements over extended temperature and lithium concentration ranges. For all samples and temperatures, the ^7Li T_1 value was calculated using only one exponential function.

Ionic Conductivity. The alternating current (ac) and direct current (dc) conductivity measurements were carried out using a Solartron impedance analyzer 1260 controlled by programmed software that operates in the $1-10^7$ Hz frequency range. The samples were monolithic pieces of about 0.5 mm thickness with flat surfaces, and the contacts were made with circular brass plates of about 0.2 cm^2. The temperature-dependent ac and dc conductivity measurements were carried out using a Janis cryostat and an oven under vacuum in the temperature range between −25 and 100 °C. Complementary dc measurements were performed using a Keithley 236 voltage source unit and were found to be in perfect agreement with those carried out with Solartron analyzer.

The room-temperature dc conductivity measurements as a function of [O]/[Li] were carried out using the same impedance analyzer; however, the contacts were made with plasticized conductivity probes (altoflex) pressed on the samples.

Differential Scanning Calorimetry (DSC). DSC measurements were performed on several 10-mg samples with a scan rate of 10 °C/min from −80 to 0 °C using a TA Instruments model 2910 differential scanning calorimeter. The glass transitions observed by DSC are taken as the inflection point of these thermograms and denoted T_g^{DSC}.

NMR Background

The line width and spin−lattice relaxation solid-state NMR measurements as a function of temperature yield information on the Li^+ (^7Li) and polymer dynamics (^{13}C) because of the motion-dependent anisotropic nuclear spin interactions. Two important parameters are obtained directly from NMR measurements of the solid polymer electrolytes as a function of the temperature. The first parameter is the temperature at which the NMR line width undergoes the narrowing phenomenon. The line narrowing indicates the occurrence of low-frequency motions (1−100 kHz) that modulate the longitudinal local fields, leading to an average of the nuclear spin interactions. The line width transitions are then commonly associated with the increase in chain motion that occurs near the temperature of the polymer glass transition, T_g. However, the agreement of T_g values from different methods is poor, and the fact that they occur at about the same temperature can be coincidence. Part of this difficulty is due to the large difference in frequencies at which the information is obtained[28−30] and how this parameter is defined from the thermograms and NMR line width measurements. For this reason, T_g^{NMR} will be used here to refer to the temperature at which the strongest change in NMR line width occurs.

The second piece of information is provided by the spin−lattice relaxation rate, T_1^{-1}, which reaches a maximum that is generally measured at a higher temperature ($> T_g^{NMR}$). This temperature, which will be denoted T_{max}, corresponds to the condition where the transverse local field fluctuations achieve sufficient amplitude at the Larmor frequency to maximize the spin−lattice relaxation rate.

The activation energy, E_a, is an important dynamical parameter that can be indirectly obtained from the NMR data. This parameter can be estimated using the Bloembergen, Purcell, and Pound (BPP) model[31−34] and the Arrhenius law. Using well-known procedures for the determination of the activation energy,[35−37] this parameter can be evaluated for both relaxation processes (line width or transversal relaxation and spin−lattice relaxation).

Ionic Conductivity Background

Direct current (dc) ionic conductivity measurements of polymer electrolytes are normally used because of the facility in following the usual abrupt conductivity transient that occurs around the polymer glass transition. The fittings of the temperature-dependent conductivity are done by the Vogel−Tamman−Fülcher (VTF) equation.[38] However, a clear picture of the microscopic conduction mechanism of the highly disordered structure of the ormolytes is better described by the random free energy barrier (RFEB) model.[39−41] This model considers the blend matrix as an isotropically disordered medium in which Li^+ ions have a considerable mobility and the alternating current (ac) conduction occurs via a hopping mechanism among ion sites. In this picture, the ions jump over energy barriers that are randomly distributed in the material bulk, the mobility being

(27) Slichter, C. P. *Principles of Magnetic Resonance*, 3rd ed.; Springer-Verlag: Heidelberg, Germany, 1990; Vol. 1.

(28) Komoroski, R. A. *High-Resolution NMR Spectroscopy of Synthetic Polymers in Bulk*; VCH Publishers: New York, 1986; Vol. 7.

(29) Frank, H. P. *Polypropylene*, 1st ed.; Gordon and Breach Science Publishers: New York, 1968; Vol. 2.

(30) Rubin, I. D. *Poly(1-butene)−Its Preparation and Properties*, 1st ed.; Gordon and Breach Science Publishers: New York, 1968; Vol. 1.

(31) Bloembergen, N.; Purcell, E. M.; Pound, R. V. *Phys. Rev.* **1948**, *73*, 679−712.

(32) Gutowski, H. S.; Pake, G. E. *J. Chem. Phys.* **1950**, *18*, 162−170.

(33) Boyce, J. B.; Huberman, B. A. *Phys. Rep.* **1979**, *51*, 189−265.

(34) Hendrickson, J. R.; Bray, P. J. *J. Magn. Reson.* **1973**, *9*, 341−357.

(35) Chung, S. H.; Jeffrey, K. R.; Stevens, J. R. *J. Chem. Phys.* **1991**, *94*, 1803−1811.

(36) Berger, S.; J, R.; Brinkmann, D.; Chowdari, B. *Solid State Ionics* **1996**, *86−88*, 475−479.

(37) Cocciantelli, J.; Suh, K.; Sénégas, J.; Doumerc, J.; Pouchard, M. *J. Phys. Chem. Solids* **1992**, *53*, 857−859.

(38) MacCallum, J. R.; Vincent, C. A. *Polymer Electrolytes Review*; Elsevier Applied Science Publishers: Essex, U.K., 1987; Vol. 1.

(39) Dyre, J. C. *J. Appl. Phys.* **1988**, *64*, 2456−2468.

(40) Bianchi, R. F.; Souza, P. H.; Bonagamba, T. J.; Panepucci, H. C.; Faria, R. M. *Synth. Met.* **1999**, *102*, 1186−1189.

(41) Bianchi, R. F.; Ferreira, G. F. L.; Lepienski, C. M.; Faria, R. M. *J. Chem. Phys.* **1999**, *110*, 4602−4607.

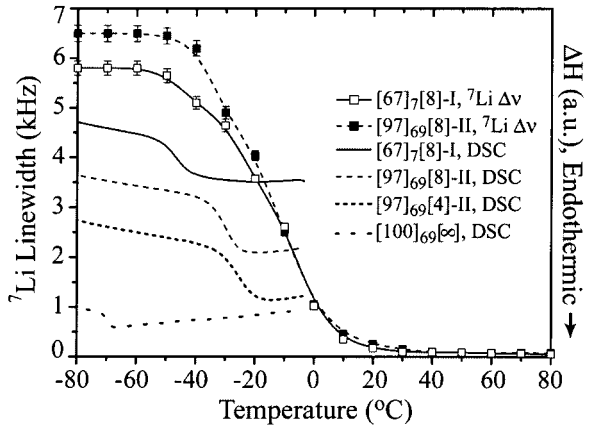

Figure 1. Temperature dependence of the ^{7}Li line width without ^{1}H decoupling for the nanocomposites belonging to series 1 and 4 in Table 1. For comparison, the corresponding DSC curves are presented with arbitrary units along the *y* axis.

dependent on the frequency of the external field. From these randomly varying free-energy barriers, RFEBs, the complex conductivity $\sigma^*(\omega)$, which predicts universal behavior independent of the temperature and of the chemical composition of the material, is obtained as

$$\sigma^*(\omega) = \frac{i\omega\sigma_0/\gamma_{\min}}{\ln\left(\frac{1 + i\omega/\gamma_{\min}}{1 + i\omega/\gamma_{\max}}\right)} - \frac{i\omega\sigma_0/\gamma_{\min}}{\ln \lambda} \qquad (1)$$

where the angular frequencies $\gamma_{\max} = \gamma_0 e^{-W_{\min}/kT}$ and $\gamma_{\min} = \gamma_0 e^{-W_{\max}/kT}$ are related to the minimum and the maximum value of the barrier energy, $W_{\min}$ and $W_{\max}$, respectively. λ is the ratio between these frequencies, i.e., $\lambda = \gamma_{\max}/\gamma_{\min}$, and $\sigma_0 = C\gamma_{\min} \ln \lambda$ is the conductivity value when the frequency goes to zero, where C is a constant depending on the density of carriers, among other parameters.

For ormolytes, two distinct activated mechanisms occurring in two different frequency ranges,[40] denoted by the indexes 1 and 2, can clearly be observed. In this case, the final equation for a $\sigma^*(\omega)$ should combine two RFEB expressions, considering that the angular frequency $\gamma_{\max 2}$ is much higher than the maximum frequency experimentally available, i.e., $\gamma_{\max 2} \gg \gamma_{\max 1}$, resulting in[40]

$$\sigma^*(\omega) = \frac{i\omega\sigma_0/\gamma_{\min 1}}{\ln\left(\frac{1 + i\omega/\gamma_{\min 1}}{1 + i\omega/\gamma_{\max 1}}\right)} - \frac{i\omega\sigma_0/\gamma_{\min 1}}{\ln(\gamma_{\max 1}/\gamma_{\min 1})} + \frac{i\omega\sigma_0/\gamma_{\min 2}}{\ln(1 + i\omega/\gamma_{\min 2})} \qquad (2)$$

It is important to note that this approximate equation remains valid over a wide range of frequencies and that the parameter γ has the dimensions of angular frequency.

Results

DSC and Ionic Conductivity. The DSC measurements for the samples [100]$_{69}$[∞], [67]$_7$[8]-I, [97]$_{69}$[4]-II, and [97]$_{69}$[8]-II are shown in Figure 1. These DSC curves show the presence of glass transitions for the four samples listed above. Table 2 summarizes the glass transition temperatures obtained from the DSC measurements for these samples.

Table 2. Glass Transition Temperatures Obtained from DSC and ^{7}Li NMR Experiments

sample	T_g^{DSC} (°C)	T_g^{NMR} (°C)
[67]$_7$[8]-I	−47.0 ± 0.5	−13.0 ± 0.5
[95]$_{34}$[4]-II	−	10.0 ± 0.5
[95]$_{34}$[8]-II	−	0.0 ± 0.5
[95]$_{34}$[15]-II	−	−12.0 ± 0.5
[97]$_{69}$[4]-II	−25.0 ± 0.5	20.0 ± 0.5
[97]$_{69}$[8]-II	−30.0 ± 0.5	−10.0 ± 0.5
[100]$_{69}$[∞]	−69.0 ± 0.5	−

Thermal properties of siloxane−PEG nanocomposites were previously studied.[13,22] Generally, the T_g^{DSC} of type I ormolytes increases with increasing polymer chain length. Unlike type I materials, type II materials show some decrease in T_g^{DSC} when the polymer chain length increases. Similarly to silica-free polymer electrolytes,[42] type I and II nanocomposites exhibit an increase in the glass transition temperature with increasing lithium concentration. However, this behavior is less accentuated for nonbonded materials. T_g^{DSC} slightly decreases with, or is not affected by, an increase in the weight percent of the polymer. For similar compositions, T_g^{DSC} values are always higher for type II materials, which is a consequence of the polymer motional hindrance introduced by the covalent bonds between the organic and inorganic phases.

These T_g^{DSC} trends were also corroborated by the ionic conductivity measurements.[15,16] For both types of ormolytes, increasing X leads to some increase in the ionic conductivity. Increasing the polymer chain length, n, decreases the ionic conductivity for the nonbonded ormolytes but increases the ionic activity for the bonded nanocomposites.

The changes in the glass transition temperatures as functions of the compositional parameters for the siloxane−PPG ormolytes display similar trends, shown in Figure 1 and Table 2, as will be discussed in the forthcoming sections. In particular, the glass transition temperatures of siloxane−PPG ormolytes are slightly displaced to higher values when the polymer rigidity is increased through a decrease of the [O]/[Li] ratio or the presence of covalent bonds (Table 2). The T_g^{DSC} values increase for both type I and II hybrids when compared to that of the nonlithiated silica-free sample [100]$_{69}$[∞], and the T_g^{DSC} values for type II materials are systematically higher than those for type I nanocomposites as a result of the covalent bonds.

Figure 2 presents the variation of the room-temperature dc conductivity as a function of [O]/[Li] for both type I (series 1) and type II (series 3) samples. These two curves present similar shapes, with maxima for the dc ionic conductivity for [O]/[Li] values of around 8 and 15 for series 1 and 3, respectively. This conductivity behavior as a function of the [O]/[Li] ratio was previously reported for siloxane−PEG ormolytes[15,16] and silica-free polymeric ionic conductors.[38,43]

(42) Roux, C.; Gorecki, W.; Sanchez, J. Y.; Jeannin, M.; Belorizky, E. *J. Phys.: Condens. Matter* **1996**, *8*, 7005−7017.
(43) Julien, C.; Nazri, G. A. *Solid State Batteries: Materials Design and Optimization*, 1st ed.; Kluwer Academic Publishers: Norwell, MA, 1994.

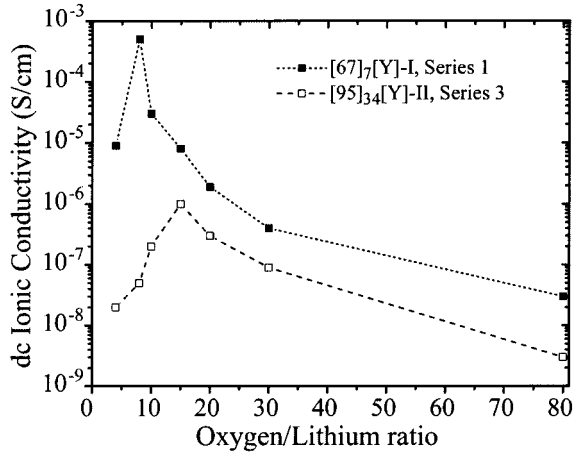

Figure 2. Behavior of the room-temperature dc ionic conductivity as a function of Y=[O]/[Li] for nonbonded (series 1, Table 1) and bonded (series 3, Table 1) samples. The uncertainties in the dc ionic conductivities are lower than 5%.

Table 3. ^{7}Li Line widths and Activation Energies Obtained from ^{7}Li Linewidth (lw) and Spin−Lattice (sl) Measurements

sample	$\Delta\nu$ (Hz)	$\Delta\nu_{dec}$ (Hz)	E_a,lw(eV)	E_a,sl(eV)
$[67]_7$[8]-I	5800 ± 100	540 ± 10	0.86 ± 0.03	0.34 ± 0.02
$[74]_5$[4]-II	5300 ± 100	310 ± 10	−	−
$[95]_{34}$[4]-II	6250 ± 100	400 ± 10	0.60 ± 0.03	0.26 ± 0.02
$[95]_{34}$[8]-II	6200 ± 100	350 ± 10	0.53 ± 0.03	0.31 ± 0.02
$[95]_{34}$[15]-II	6100 ± 100	310 ± 10	0.42 ± 0.03	0.31 ± 0.02
$[97]_{69}$[4]-II	6100 ± 100	420 ± 10	0.77 ± 0.03	0.29 ± 0.02
$[97]_{69}$[8]-II	6500 ± 100	360 ± 10	0.54 ± 0.03	0.31 ± 0.02
$[97]_{69}$[15]-II	6400 ± 100	310 ± 10	0.41 ± 0.03	0.26 ± 0.02

Important aspects of ionic conductivity associated with the heterogeneous composition of ormolytes are discussed in the following sections.

^{7}Li and ^{13}C NMR Spectroscopies. Below the glass transition, the 2-T ^{7}Li spectra consist of a very intense central transition ($-^1/_2 \leftrightarrow +^1/_2$), whose width is predominately due to ^{1}H−^{7}Li dipolar interactions as confirmed by proton-decoupling experiments (Table 3), and also a broad (∼10−30 kHz) line that could be associated with quadrupolar satellite transitions ($^3/_2 \leftrightarrow {}^1/_2$ and $-^1/_2 \leftrightarrow -^3/_2$). When the temperature is increased, both the narrow and broad lines are narrowed around the glass transition temperature. The presence of the quadrupolar satellite transitions below T_g was confirmed by solid-echo experiments performed at 9.4 T and by the fact that this line is not affected by the utilization of proton decoupling. A clear example of a ^{7}Li spectrum consisting of both central and satellite transitions is shown in Figure 3 at a temperature well below the glass transition temperature (T = −100 °C) for the sample $[97]_{69}$-[8]-II (see Table 2). Because the ormolytes are heterogeneous systems, it is expected that they present a wide distribution of electric field gradients, which results in a Gaussian-broadened satellite line. The magnitude of the electric quadrupole coupling constant is estimated from the ^{7}Li 9.4-T solid-echo experiments to be ca. 26 kHz at −100 °C (Figure 3). Because this work was based mostly on the 2-T ^{7}Li spectra, where it is relatively difficulty to analyze the quadrupolar satellite transitions observed below and around the glass transition, only the 2-T ^{7}Li central transitions were investigated in detail.

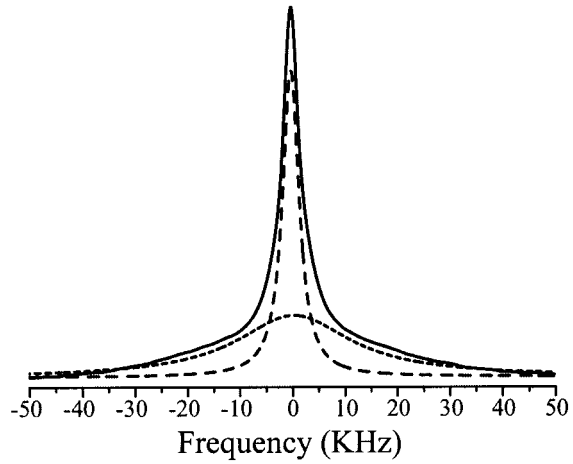

Figure 3. Typical low-temperature (T = −100 °C, $T < T_g$) ^{7}Li spectrum for ormolytes (solid line) obtained employing solid-echo at 9.4 T and 384 scans using the sample $[97]_{69}$[8]-II. The long- and short-dashed lines correspond to the deconvolution of the experimental spectrum in the central (narrow) and satellite (broad) transitions, respectively.

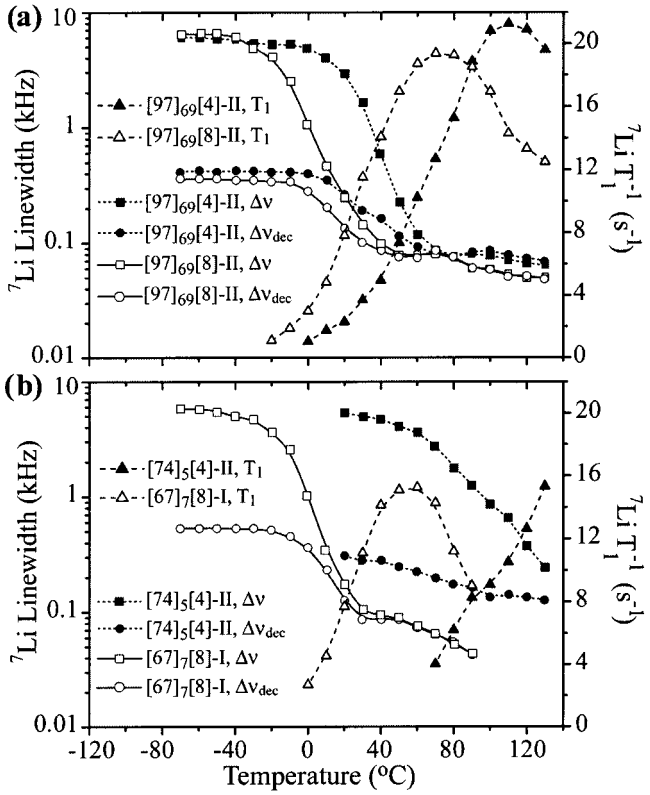

Figure 4. Temperature dependence of the ^{7}Li spin−lattice relaxation rate and line width, with and without ^{1}H decoupling, for the nanocomposites (a) $[97]_{69}$[4]-II and $[97]_{69}$[8]-II and (b) $[67]_7$[8]-I and $[74]_5$[4]-II. The uncertainties in the ^{7}Li spin−lattice relaxation rates and line widths are lower than 5%.

The 2-T ^{7}Li line width, measured with and without ^{1}H decoupling, and the spin−lattice relaxation time of the central transition were investigated as functions of temperature from −100 to 140 °C for several samples listed in Table 1.

Typical results from these measurements can be seen in Figures 1 and 4 for both type I and II nanocomposites. In Figure 1, the ^{7}Li line width is plotted using a linear y scale to show the direct effect of the glass transition

Table 4. T_{max} Temperatures and the Corresponding ^{7}Li Spin−Lattice Relaxation Rates

sample	T_{max} (°C)	$(1/T_1)_{max}$ (s^{-1})
$[67]_7$[8]-I	55 ± 1	15.0 ± 0.5
$[95]_{34}$[4]-II	91 ± 1	18.0 ± 0.5
$[95]_{34}$[8]-II	90 ± 1	18.5 ± 0.5
$[95]_{34}$[15]-II	89 ± 1	20.5 ± 0.5
$[97]_{69}$[4]-II	110 ± 1	21.5 ± 0.5
$[97]_{69}$[8]-II	76 ± 1	19.5 ± 0.5
$[97]_{69}$[15]-II	74 ± 1	20.0 ± 0.5

observed by DSC on the ^{7}Li line narrowing. In contrast, in Figure 4, it is plotted using a logarithmic *y* scale to show the small ^{7}Li line width broadening observed around T_{max} . The curves for the different materials of each series present similar shapes, but the characteristic parameters T_g^{NMR}, T_{max} , and line widths vary.

Taking Figure 1 as an example, the ^{7}Li line width evolution with temperature for siloxane−PPG ormolytes can be described by a curve composed of two plateaus separated by a temperature range where rapid changes in line width occur. As can be seen, the central line width transitions occur at temperatures similar to the glass transition temperatures observed by DSC; they are taken as the inflection points of these line width curves measured without ^{1}H decoupling and denoted T_g^{NMR}. These characteristic glass transition temperatures for the siloxane−PPG hybrids are in the range between −13 and 20 °C and are summarized in Table 2. Below T_g^{NMR}, the polymer is rigid, and the rigid-lattice line widths are denoted $\Delta\nu$ or $\Delta\nu_{dec}$ when measured without or with proton decoupling, respectively (Table 3).

An additional broadening of the ^{7}Li line can also occur because of the finite life of the spins in any eigenstate as a result of the spin−lattice relaxation,[27] and this effect should be evident around T_{max} . In this situation, the spin−lattice relaxation rates can reach values on the order of ^{7}Li line width, introducing a nonsecular line broadening. To estimate the lifetime broadening contribution to the ^{7}Li line width, the temperature dependence of the ^{7}Li spin−lattice relaxation rate of the central transition, T_1^{-1}, is also shown in Figure 4. These bell-shaped curves present maxima $(1/T_1)_{max}$ at temperatures T_{max} above 50 °C (Table 4) and indicate a small nonsecular broadening contribution to the ^{7}Li line width (Figure 4).

The activation energies were calculated for both relaxation processes (Table 3).[35−37] In the case of line width, the activation energies were obtained from the ^{7}Li measurements performed without proton decoupling around the glass transition. In the case of spin−lattice relaxation, the values of the activation energies were found in the temperature interval below T_{max}.

The effects of the compositional parameters *X*, *Y*, *n*, and *Z* on the NMR parameters T_g^{NMR}, T_{max} , $\Delta\nu$, $\Delta\nu_{dec}$, $(1/T_1)_{max}$, and E_a are summarized in Tables 2−4, and their trends will be discussed in the forthcoming sections.

To estimate the contribution of the polymer chain (PPG) to the ion dynamics, ^{13}C NMR experiments were also performed, involving line width measurements as a function of temperature. Ormolytes of both types I and II, namely, $[67]_7$[8]-I, $[97]_{69}$[4]-II, and $[97]_{69}$[8]-II, were studied. These data are presented in Figure 5, together

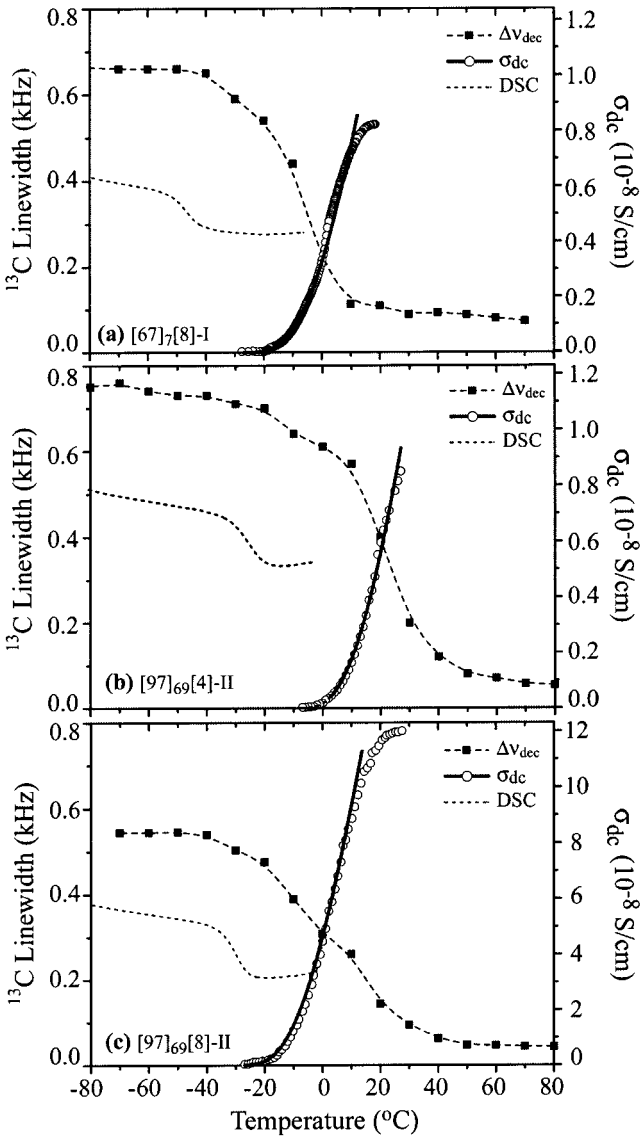

Figure 5. Temperature dependence of ^{13}C line width for (a) $[67]_7$[8]-I, (b) $[97]_{69}$[4]-II, and (c) $[97]_{69}$[8]-II. For comparison, the DSC (presented without a *y* scale) and dc ionic conductivity are presented for all samples. The uncertainties in the ^{13}C line widths are approximately 5%, and those in the dc conductivity are lower than 5%. Fittings of the temperature-dependent conductivity measurements were made by using the Vogel−Tamman−Fülcher model (solid lines).

with the dc ionic conductivity and DSC measurements, to facilitate the comparison between the polymer dynamics and the ionic conductivity.

Ionic Conductivity versus Frequency: Random Free Energy Barrier Model

Figure 6 shows the real part of the ac conductivity of the sample $[97]_{69}$[8]-II at different temperatures. At −23 °C, the conductivity increases slowly at low frequencies, exhibiting a faster increase above 1 kHz. Between −23 and 4 °C, an abrupt enhancement in the conductivity is observed, in agreement with that recorded in dc measurements. At 4 °C, the real conductivity exhibits a plateau below 10^4 Hz, followed by a linear increase on the log−log scale. Above 4 °C, a plateau between two inflection points in the conductivity curve can be observed. Considering the RFEB model, this result

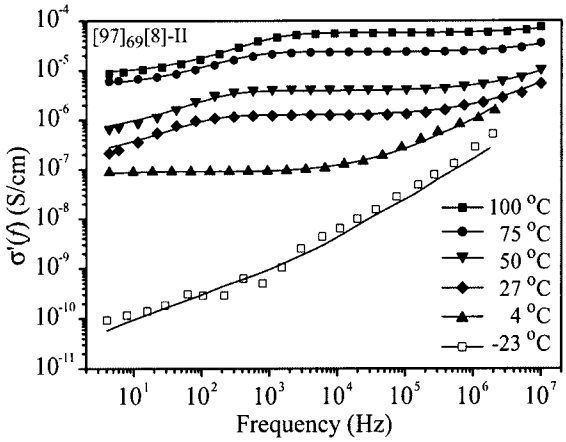

Figure 6. Real component of ac conductivity $\sigma'(f)$ carried out with sample $[97]_{69}[8]$-II at several temperatures. Fittings of the experimental curves (continuous lines) were done by using eq 2.

indicates that there is more than one hopping mechanism. Equation 2 was used to fit with good accuracy the experimental results of Figures 6 and 7, which presents both the real and the imaginary components of the complex conductivity measured at 75 °C for the samples $[97]_{69}[8]$-II, $[97]_{69}[15]$-II, and $[97]_{69}[30]$-II. The parameters obtained from the fittings are summarized in Tables 5 and 6.

Although a bulk hopping transport mechanism in the low-frequency region was assumed, the electrode/electrolyte interfacial phenomena including surface roughness and the possibility of some slow electrode reactions under an applied electric field are not discarded.

Discussion

Polymer−Cation and Polymer−Siloxane Interactions. The ^{7}Li line width was measured as a function of temperature for several samples listed in Table 1. The results show that, independent of the decoupling condition, the line width transitions occur near the glass transition temperatures of the nanocomposites (Figure 1). Furthermore, the ^{13}C NMR measurements performed on the three samples $[67]_7[8]$-I, $[97]_{69}[4]$-II, and $[97]_{69}[8]$-II show line width glass transitions starting at temperatures very similar to those measured for the cation Li^+ (Figure 5). Therefore, rapid cation motion and, consequently, higher ionic conductivity occurs only when the polymer segments motions are large enough to assist the cationic jumps.[10,15,23,44−46]

In the rigid-lattice regime, the ^{7}Li line widths obtained with and without ^{1}H decoupling (Table 3) demonstrate that the ^{7}Li−^{1}H magnetic dipolar interaction accounts for approximately 90% of the ^{7}Li spin interactions. Around T_{max}, a slight modification of the ^{7}Li line width with temperature is observed in several samples (Figure 4). This is a consequence of the high spin−lattice relaxation rates reaching average values of 19 ± 1 Hz (Table 4), which are on the order of the line width around T_{max} .

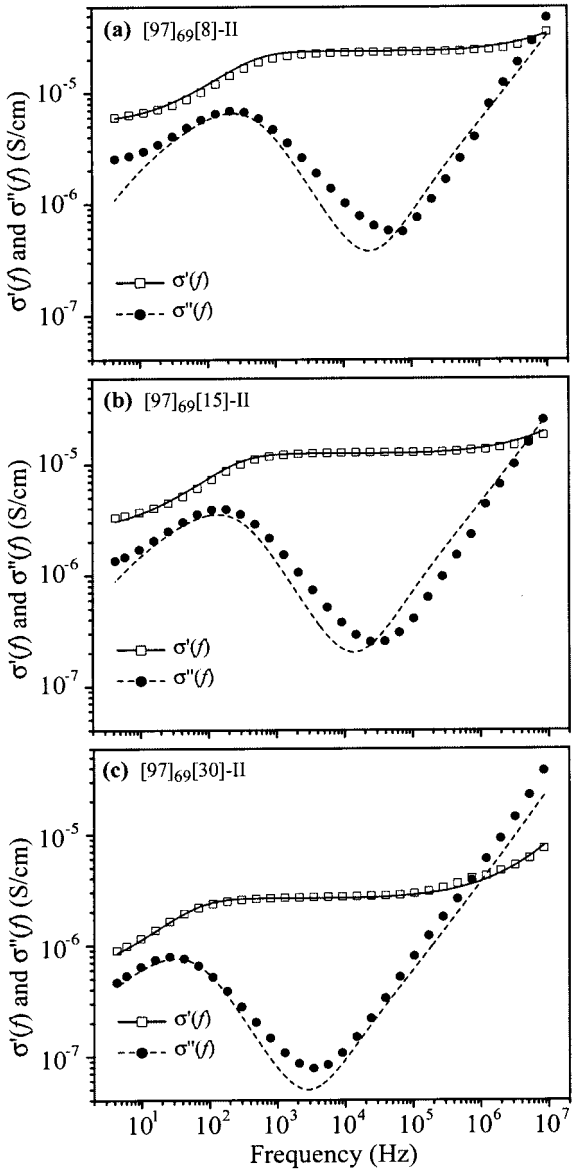

Figure 7. Real $\sigma'(f)$ and imaginary $\sigma''(f)$ components of ac conductivities of samples (a) $[97]_{69}[8]$-II, (b) $[97]_{69}[15]$-II, and (c) $[97]_{69}[30]$-II at 75 °C. Fittings of the experimental curves (continuous and dashed lines) were done by using eq 2.

Table 5. Parameters Obtained by Fitting the Curves of Figure 6 Using Eq 2

T (°C)	σ_0(S/cm)	$\gamma_{min1}/2\pi$ (Hz)	$\gamma_{max1}/2\pi$ (Hz)	$\gamma_{min2}/2\pi$ (Hz)
100	4.7×10^{-6}	4.4	1800	2.7×10^5
75	2.8×10^{-6}	3.0	660	1.7×10^5
50	2.9×10^{-7}	0.7	310	1.7×10^4
27	1.2×10^{-7}	0.4	30	6.3×10^3
4	3.5×10^{-8}	0.2	5	7.5×10^2
−23	1.0×10^{-8}	−	−	−

Table 6. Parameters Obtained by Fitting the Curves of Figure 7 Using Eq 2

T (°C)	σ_0(S/cm)	$\gamma_{min1}/2\pi$ (Hz)	$\gamma_{max1}/2\pi$ (Hz)	$\gamma_{min2}/2\pi$ (Hz)
$[97]_{69}[8]$-II	2.8×10^{-6}	3.0	6.6×10^2	1.7×10^5
$[97]_{69}[15]$-II	1.3×10^{-6}	1.3	3.3×10^2	1.4×10^5
$[97]_{69}[30]$-II	2.9×10^{-7}	0.3	8.5×10^1	1.0×10^4

Judging from the above discussion, the polymer dynamics and the Li^+ ion motion or diffusion cause the observed temperature dependence of both the ^{7}Li line width and the spin−lattice relaxation time. Also, the ^{1}H−^{7}Li interaction is predominately responsible for the

(44) Arumugam, S.; Shi, J.; Tunstall, D. P.; Vincent, C. A. *J. Phys.: Condens. Matter* **1993**, *5*, 153−160.
(45) McLin, M. G.; Angell, C. A. *J. Phys. Chem.* **1996**, *100*, 1181−1188.
(46) Müller-Plathe, F.; van Gunsteren, W. F. *J. Chem. Phys.* **1995**, *103*, 4745−4756.

temperature behavior of the ^{7}Li line width. However, some studies[35] indicate that the quadrupolar interaction is responsible for the ^{7}Li spin−lattice relaxation. The minimum ^{7}Li T_1 values obtained for all samples are very similar, showing an average value of 52 ± 3 ms (Table 4). This fact indicates that the quadrupolar couplings and the ^{7}Li sites are also very similar for all of the samples.

The activation energies obtained from the curves of the ^{7}Li line width and spin−lattice relaxation for several ormolytes (Table 3) have values similar to those found for silica-free ionic conducting polymers.[35] It is important to note that the activation energies obtained from line width measurements are perceptibly larger than those obtained from spin−lattice relaxation measurements. These results indicate that a single relaxation model BPP cannot be used along the whole temperature interval. This result is reasonable because the activation energy necessary for the glass transition process is expected to be larger than that for the hopping process of the cation Li^+ above T_g.[35]

Influence of the Compositional Parameters. The major trends of the ^{7}Li NMR spectral changes as a function of the compositional parameters are summarized in Tables 2−4 and Figures 1, 4, and 5. The following general evidence is observed in these tables and figures.

(1) Comparison between Siloxane−PPG and Siloxane−PEG Ormolytes. The NMR and DSC measurements shown in Figures 1 and 5 and ref 22 indicate that the siloxane−PPG and siloxane−PEG nanocomposites exhibit similar behaviors. For both ormolytes, the motion in the polymer chain provides an intense increase in the ionic conductivity above the glass transition temperature.

(2) Effects of the Lithium Concentration (Y) on Type II Ormolytes. As observed before for siloxane−PEG bonded ormolytes,[22] the effect of increasing the lithium concentration on type II siloxane−PPG hybrids (series 3) results in an expected increase for T_g^{NMR} and T_{max} of tens of degrees Celsius (Figure 4a). This observation is corroborated by the plots of dc conductivity versus temperature shown in Figure 5b and c, where the earlier increase of σ_{dc} for the sample with lower lithium content ($[97]_{69}$[8]-II) can be observed.

(3) Effects of the Interactions between the Polymer and the Inorganic Phase. Figure 4b presents the temperature dependence of the ^{7}Li line width without ^{1}H decoupling and the ^{7}Li spin−lattice relaxation rate for the nonbonded and bonded nanocomposites $[67]_7$[8]-I and $[74]_5$[4]-II, respectively, which have similar X, n, and Y parameters. The effect of the covalent bonding of the polymer chain to the inorganic silica structure (sample $[74]_5$[4]-II) is clearly apparent from the ^{7}Li line width and spin−lattice relaxation data, which show a large shift of the T_g^{NMR} and T_{max} values toward higher temperatures relative to those of the type I ormolyte (sample $[67]_7$[8]-I).

This result is consistent with the ionic conductivity measurements (Figure 2), which present systematically lower conductivity values for bonded ormolytes compared with the nonbonded materials of similar compositions. This confirms that the presence of covalent bonds between the silica structure and the PPG chains strongly hinders the polymer motion and consequently the Li^+ mobility, leading to an increase of T_g^{NMR} and a decrease of ionic conductivity. This interpretation is also confirmed by DSC measurements, which show that the T_g^{DSC} value of the nonbonded sample $[67]_7$[8]-I is much lower than those of the bonded samples $[97]_{69}$[4]-II and $[97]_{69}$[8]-II, revealing a much lower mobility of polymer chains in type II nanocomposites for similar temperatures.

Conclusions

The dissolution of $LiClO_4$ into nanocomposites consisting of PPG and siloxane phases provides materials with ionic conductivities that could reach values comparable to those of pure polymer electrolytes. In addition, the much better mechanical properties and transparency of these hybrids compared to those of pure PPG, a viscous liquid at room temperature, allows their possible use in electrochromic or photoelectrochemical devices, batteries, and sensors.[4−7,9−11]

NMR, ionic conductivity, and DSC studies were performed to probe specifically the behavior of both the mobile cations and the polymer chains for type I and II siloxane−PPG ormolytes. These combined experiments demonstrate that the thermal and electrical behavior of such solid electrolytes strongly depends on the mobility of these species. Furthermore, as observed for pure organic ion-conducting polymers, conductivity is promoted by the segmental motion of the polymer chains.

The temperature dependence of the dc ionic conductivity follows the VTF model, and the random free energy barrier model (RFEB) explains the ac hopping mechanism with good accuracy. The RFEB model also explains the ac ionic conductivity in such composites, which is in agreement with their disordered and heterogeneous structure.

Acknowledgment. The authors thank Prof. G. F. Leal Ferreira for the helpful discussions about conductivity and M. L. Simões for helping in the sample preparation. The Brazilian Agencies FAPESP, CNPq, and FINEP and the Brazil−France Project USP-COFECUB supported this research.

CM011023V